



Effects on APC antigen presenting cells of short-term interaction with the human human host defense peptide beta-defensin 2

Francesca Morgera, Sabrina Pacor, Luisa Creatti, Nikolinka Antcheva, Lisa Vaccari, Alessandro Tossi

► To cite this version:

Francesca Morgera, Sabrina Pacor, Luisa Creatti, Nikolinka Antcheva, Lisa Vaccari, et al.. Effects on APC antigen presenting cells of short-term interaction with the human human host defense peptide beta-defensin 2. *Biochemical Journal*, 2011, 436 (3), pp.537-546. 10.1042/BJ20101977 . hal-00596262

HAL Id: hal-00596262

<https://hal.science/hal-00596262>

Submitted on 27 May 2011

HAL is a multi-disciplinary open access archive for the deposit and dissemination of scientific research documents, whether they are published or not. The documents may come from teaching and research institutions in France or abroad, or from public or private research centers.

L'archive ouverte pluridisciplinaire **HAL**, est destinée au dépôt et à la diffusion de documents scientifiques de niveau recherche, publiés ou non, émanant des établissements d'enseignement et de recherche français ou étrangers, des laboratoires publics ou privés.

Effects on antigen presenting cells of short-term interaction with the human host defense peptide beta-defensin 2

Francesca Morgera^{*†}, Sabrina Pacor^{*}, Luisa Creatti^{*}, Nikolinka Antcheva^{*}, Lisa Vaccari[†], Alessandro Tossi^{*2}

^{*}Department of Life Sciences, University of Trieste, Trieste, 34127, ITALY and

[†]ELETTRA Synchrotron Light Laboratory, Basovizza, Trieste, 34149, ITALY.

Abstract

β -Defensins are antimicrobial peptides that exert their host-defense functions at the interface between the host and microbial biota. They display a direct, salt and medium sensitive cidal activity, *in vitro*, against a broad spectrum of bacteria and fungi and there is increasing evidence that they also play a role in alerting and enhancing cellular components of innate and adaptive immunity. Their interaction with biological membranes plays a central role in both these types of activities. In this study we have investigated the interaction of fluorescently labelled human β -defensin 2 (hBD2) with monocytes, macrophages and immature dendritic cells, observing a differential capacity to be rapidly internalised into these cells. Complementary microscopy techniques (TEM, optical and infrared) were used to explore the functional and biological implications of these interactions on immature dendritic cells. Short-term exposure to the peptide resulted in significant alterations in membrane composition and re-organization of the endomembrane system, with induction of degranulation. These events may be associated with the antigen-presenting activities or the chemotaxis of iDC, which appears to occur via both CCR6-dependent and independent mechanisms.

Keywords: beta-defensin / host defense / innate immunity / chemotaxis / membrane interactions / infrared microspectroscopy.

INTRODUCTION

Mammalian β -defensins (BD) are small, cationic host-defence peptides (HDPs) with a characteristic β -sheet fold that exert their protective functions at the host-environment interface [1]. They were initially proposed to act as innate immune effectors by a direct, antibiotic-like activity [2] but more recently a complex, sophisticated and possibly more relevant role in infection has emerged, as signal molecules alerting and/or activating cellular components of both innate and adaptive immunity [3-4].

Humans possess two related defensin families, with similar folds but with differing disulphide bridging patterns; α -defensins are expressed in neutrophils, certain macrophages and Paneth cells, whereas β -defensins are mostly produced by epithelial cells lining different organs, such as epidermis, the bronchial tree and the genitourinary tract [2]. While some are produced constitutively, more often they are induced by microbial products or proinflammatory cytokines. They generally display a salt-sensitive antimicrobial activity *in vitro*, against a broad spectrum of bacteria, fungi and some enveloped viruses [5]. *In vivo*, they are likely to be secreted into the phagocytic vacuoles of phagocytes and/or on epithelial surfaces and mucosa, where the ionic strength is relatively low, reaching sufficiently high concentrations for antimicrobial activity.

Defensins are not cytotoxic to host cells at antimicrobial concentrations, and this selectivity may depend on the different compositions of cellular membranes; in the case of bacteria, the greater abundance of negatively charged phospholipids and the lack of cholesterol may favor the membrane as a target. The mechanism by which bacteria are inactivated by defensins is however not well understood. Conversely, human β -defensins alert cellular components of both the innate and adaptive immune systems, and enhance the activities, without membrane damage [1]. hBD2 is the best characterized in this respect: it induces activation and degranulation of mast cells with release of histamine and prostaglandins, thus favoring the recruitment of neutrophils to the inflammatory site. Moreover, it displays a chemotactic activity for CD8⁺ T cells, immature dendritic cells, as well as TNF- α -activated neutrophils and epithelial cells and triggers a robust production of cytokines from PBMC [6-11]. hBD2 also inhibits the classical pathway of the complement system, suggesting a protective role against its uncontrolled activation [12].

The overall picture that is emerging on the role of defensins *in vivo* is that they act in an articulated and quite complex manner, by directly contrasting invading microorganisms, by recruiting PMN, T-cells and immature dendritic cells (iDC) to the site of infection, and as enhancers or regulators of inflammatory and/or healing responses. It suggests that this class of HDPs may lead to promising leads for the future development of multifunctional anti-infective agents and/or vaccine adjuvants. Many of the reported biological functions are however based on phenomenological observations *in vitro*, and important questions remain to be answered regarding the underlying mechanisms before the *in vivo* relevance in host defence can be assessed.

In this study several different techniques were used to investigate the consequences of short-term (30-60 min) interaction between hBD2 and antigen presenting cells. Flow cytometry and confocal microscopy were used to determine whether fluorescently labelled hBD2 localised exclusively at the membrane level or also intracellularly in macrophages, monocytes or immature dendritic cells. Focusing then on its interaction with immature dendritic cells, the functional and biological implications were explored by using complementary microscopy techniques. In

particular, Synchrotron Radiation Infrared MicroSpectroscopy (SR-IRMS) was used to observe biochemical changes in macromolecular constituents of hBD2-treated cells. SR-IRMS is a label-free and non-destructive micro-analytical tool for the characterization of molecular modes of vibrations, and was employed for typifying cellular samples, through correlation with their morphological features. The high brilliance of SR was exploited to achieve cellular and sub-cellular spatial resolution [13]. Analysis of band shape, position and intensity revealed subtle biochemical changes, relating to membrane composition and order [14], or protein and nucleic acid structure [15,16]. Distinct subsets of cells with different responsiveness to peptide treatment were clearly identified, in agreement with flow cytometry, and suggested that the effects of exposure to hBD2 included potential variations in cellular protein content and lipid/phospholipid distributions. These effects were considered also in relation to known activities of the peptide, such as the chemotactic effect on iDC.

MATERIALS AND METHODS

Peptide synthesis and characterization.

hBD2 was synthesized by the Fmoc-solid phase method using 2-chlorotrityl chloride resin (substitution ≤ 0.2 mmol/g), and after cleavage the crude peptide was of sufficiently good quality to be directly oxidatively folded for 24h in N₂-saturated aqueous buffer (0.1 M ammonium acetate pH 7.8, containing 0.5M guanidinium HCl and 2 mM EDTA) in the presence of 100 fold excess of cysteine and 10 fold excess of cystine with respect to the peptide, as described in more detail in the supplementary material. Monitoring by analytical RP-HPLC and ESI-MS, confirmed completion, and final purification was carried out on a preparative C18 column. 5(6)-carboxyfluorescein (CF) labeling at the free N-terminal position of hBD2 (CF-hBD2) was carried out on resin-bound, fully side-chain protected peptide prior to cleavage and folding, while that with BODIPY (BY-hBD2) was carried out on folded peptide, as this molecule is not stable to cleavage conditions (see Supplementary material). The complete oxidation and correct labeling was verified by ESI-MS of the peptide, while correct folding was partly confirmed by ESI-MS analysis of proteolytic digests. Unlabelled peptide concentrations were determined based on the molar extinction coefficients (ϵ_{280}) of Tyr and Cys, while labelled peptides based on the extinction coefficients of CF or BY respectively. Peptide stock solutions (~ 100 μ M in MQ water) were determined to be LPS-free by the LAL assay (Bio-Whittaker U.S.A).

Cellular uptake of hBD2

Cells were resuspended in complete medium at 1×10^6 /ml and incubated at 37°C in the presence of CF- or BY-hBD2 for defined periods before cytofluorimetric analysis. The fluorescent signal from total bound peptide (on the cellular membrane and/or internalized into cells) was acquired first. Treated cells were then incubated with 0.1% trypan blue (TB), which quenched peptide bound to the external membrane surface only, as it is excluded from the interior of intact cells. Permeabilization of cells by hBD2 was monitored by the propidium iodide (PI) exclusion assay and the PI+ cell population, if any, was excluded from subsequent analysis. Flow cytometric analyses used a 488-nm (argon ion laser) excitation on a Cytomics FC 500 instrument (Beckman Coulter). A minimum of 10000 events per sample was acquired and histograms were analyzed with the FCS Express software (De Novo Software, CA).

The fluorescence of each sample was determined as mean fluorescence channel intensity (MFI). All experiments were carried out in triplicate and repeated at least three times. Data are expressed as mean value \pm SEM.

Generation of monocyte-derived dendritic cells (MDDCs) from peripheral blood

Monocytes were prepared from buffy coat obtained from 20 informed, healthy donors and isolated by Histopaque® density gradient centrifugation. Plastic adherent cells (monocytes) were maintained at 37°C in a humidified atmosphere of 5% CO₂ in RPMI-1640 supplemented with 10% human serum NHS, 2 mM L-glutamine, 25 mM HEPES, 100 U/ml penicillin, and 100 µg/ml streptomycin (complete medium). iDCs were induced with GM-CSF (25 ng/ml) and IL-4 (0-44 ng/ml) for 7 days [17]. These were then phenotypically characterized using antibodies for HLA-DR, CD11c, DC-SIGN, CD83, CD1b, CD14 and CCR6 as markers to confirm differentiation, as described in detail in the supplementary material. While HLA-DR, CD11c, DC-SIGN were persistently highly expressed (80-90% positive in all cell preparation), the percentage of cells positive for membrane exposed CCR6 were quite variable in different preparations (ranging from 0-70%), despite the fact that cytosolic CCR6, as revealed by treatment of cells with ethanol and saponin, was persistently highly expressed (> 90% positive cells in all preparations). This indicates that while the induction conditions were appropriate, a considerable variability occurs amongst different donors, as also reported in the literature [18]. By altering the concentration of IL-4 in the culture medium it was possible to somewhat modulate receptor exposition [19].

Cytotoxicity and effect on protein content

To take cytotoxic effects of hBD2 into account when assessing its biological activities, monocytes were incubated with increasing peptide concentrations (1-16 µM in SPB with 0-150 mM NaCl) for 30 min, at 37°C, washed, resuspended in PBS and treated with 10 µl propidium iodide (PI) solution (0.5 mg/ml in PBS) immediately prior flow cytometric analysis.

To assess the effect of hBD2 on protein content, treated and untreated iDC7 were diluted to 5×10^5 cells/ml in PBS, fixed with ice-cold 70% EtOH and stored at 4°C overnight. Cells were washed twice in PBS, centrifuged at 400 rpm at 4°C, before incubation with FITC (0.05 µg/ml) in PBS buffer. Measurements were carried out by flow cytometry as described above.

TEM analysis of iDC ultrastructure

After centrifuging, the cell pellet was fixed in 3% glutaraldehyde in 0.1 M cacodylate buffer (pH = 7.3) at 37°C for 2-3 h. The cells were post-fixed for 1 h at 4°C with 1% osmium tetroxide in 0.1 M cacodylate buffer, dehydrated in an ethanol series, and then embedded in epoxy resin. Ultra thin sections were examined after post-staining with 5% (w/v) uranyl acetate in 30% (v/v) ethanol for 20 min and Reynolds lead citrate for 5 min. on a PHILIPS EM 208 transmission electron microscope (Centro Servizi Polivalente d'Ateneo; University of Trieste, Italy).

SR-IRMS

Single whole-cell and intracellular analyses have been carried out at the infrared beamline SSSI (Synchrotron Infrared Source for Spectroscopy and Imaging) [20] at

the Elettra Synchrotron Light Laboratory in Trieste, Italy. hBD2-treated and untreated iDCs were deposited on CaF₂ IR-transparent windows and cell adhesion obtained with 30 minute incubation at 37°C. Cells were then washed with PBS and fixed in 4% formalin in PBS for 20 minutes at room temperature, a type of fixation that does not interfere significantly with IR absorbances and maintains fundamental biochemical and structural cellular aspects [21]. Washed samples were ambient dried and then stored under vacuum until FTIR measurements. Spectral data were collected in transmission mode (15X condenser-objective) using a Bruker Vertex 70 interferometer coupled with the Hyperion 3000 Visible-IR microscope, equipped with a nitrogen cooled Mercury-Cadmium-Telluride detector.

Single cells were visually selected and whole cell IR spectra were collected with at a 50×50 µm spatial resolution (minimum 30 cells per sample), in order to have information on the general state and homogeneity of the sample. Each spectrum was the average of 256 scans with 4 cm⁻¹ spectral resolution, and processed and analyzed with the OPUS 6.5 software (Bruker Optics GmbH, Ettlingen, Germany), applying a compensation algorithm correcting for atmospheric water vapor and carbon dioxide spectral contributions. Cluster analysis was then applied in the 3600-1100 cm⁻¹, 3020-2800 cm⁻¹ and 1760-1475 cm⁻¹ spectral ranges (Euclidean distances, Ward's classification algorithm), by processing vector normalized first derivatives of FTIR cell spectra to enhance spectral band resolution and minimize baseline variations, (Savitzky-Golay algorithm, 9 smoothing points). Selected iDCs were subsequently subjected to higher resolution IR mapping, with a 5×5 micron spatial resolution using a grid that matched the whole cell area and collecting an FTIR spectrum at each grid point, achieving a good compromise between S/N in the range of interest (3600-1000 cm⁻¹) and adequate spatial resolution for resolving biomolecular macro-domains. A background spectrum was recorded every 5 or 6 map points in order to correct for the SR current decay during the experiment's course. The maps were analyzed using the univariate technique of functional group mapping. The integrated bands used to generate maps were the Amide I (1707-1590 cm⁻¹) for proteins (P), the carbonyl ester band (1760-1720 cm⁻¹) for phospholipids (Ph) and the acyl chain bands (3000-2800 cm⁻¹) for lipids in general (L).

Chemotaxis assays

iDC migration was assessed *in vitro* using a Transwell chamber with 8 µm pore polycarbonate filters (Corning-Costar, USA). Cells (10⁶ /ml) were stained with FastDil dye (10 µM) for 20 min. at 37°C, thoroughly washed and resuspended in RPMI-1640, 1% BSA (chemotaxis medium) and a 100 µl suspension added to the upper compartment. Peptides (1 µM) or positive control (12.5 nM recombinant human MIP-3α (Chemicon Int., MA, USA) were then placed in the lower compartment. After 90 min incubation, both migrated and transmigrating cells were quantified fluorimetrically at 530 nm on a Packard FluoroCount instrument. Results are expressed in percentage respect to spontaneous motility of cells (migration + transmigration), in chemotaxis medium without chemokines. In some experiments, cells were pretreated with the CCR6 antibody for 30 min. to specifically inhibit receptor-mediated chemotaxis.

Confocal microscopy

APC cells were allowed to adhere on glass slides and than they were treated with CF-hBD2 (1µM) for 60 min; after washing they were fixed with PFA 3% at room

temperature for 20 min. Fixed cells were then incubated 5 min with 0.1M glycine (0.02% NaN₃) in PBS. Permeabilisation was performed with 0.01% Triton X-100 for 5 min and actin was counter-stained with Phalloidin-TRITC (SIGMA-Aldrich, Italia) for 15 min (3.8 μ M). After washing, cells were mounted with Mowiol (4-88) (Polysciences, Inc., Germany) and conserved in darkness at -20°C until microscope analysis. Cells were examined with an Eclipse C1si Nikon Instrument equipped with two detectors at standard confocal detection unit and images were elaborated by EZ-C1 software version 3.30.

RESULTS

Prior to performing analyses for hBD2 binding to and internalization into APC, we verified that it was not cytotoxic to cells of the mononuclear-phagocytic lineage (CD14+) at the concentration used, by monitoring membrane permeabilisation to propidium iodide (PI) and vitality as assessed by the MTT test. No significant toxicity was observed up to 4 μ M peptide, under any of the medium conditions used, for exposure times ranging from 0.5 to 72 hours (results not shown).

Peptide binding and internalization into APC

Macrophages derived from blood circulating monocytes (MDM) were incubated with 1 μ M carboxyfluorescein labeled hBD2 (CF-hBD2) at 37°C for increasing periods up to 24 h and analyzed by flow cytometry to confirm the ability of hBD2 to bind to the cellular membranes. Mean channel fluorescence intensity (MFI) of cells rapidly increased, indicating that hBD2 bound rapidly to the cell surface, with more than 80% of cells having bound CF-hBD2 after 10 min and all cells by 60 min (Fig. 1A), and total fluorescence remained quite constant up to 24 h. PMA-derived macrophages behaved in a similar manner (data not shown).

Treating samples with 0.1% of the impermeant quencher Trypan blue (TB) immediately prior to flow cytofluorimetric analysis allowed to selectively quench peptide externally bound to the surface, and confirm the rapid internalization of CF-hBD2 into macrophage cells (compare open bars to filled bars in Fig. 1A). At 60 min over 95% of cells were positive for the peptide with 60% of the signal persisting after TB quenching. Confocal microscopy of macrophage cells confirms that at 60 min most of the peptide fluorescence is in the cytoplasm, and distributed in a punctuate manner (Fig. 1B).

Blood derived monocytes also bound CF-hBD2 but to a lesser extent than macrophages (Fig. 1A). Overall, a 5-6 fold increase in fluorescence and 40% internalized peptide was observed for monocytes, against an 18-20 fold increase in fluorescence and 60% internalised peptide observed for macrophages. iDCs showed a considerable capacity to bind peptide (Fig. 1A, black bars), with a very strong (40-50 fold) increase in fluorescence immediately after contact with 1 μ M CF-hBD2. Fluorescence due to internalised peptide at 60 min exposure was about 35% of total, so that overall a comparable amount of peptide was internalised as for macrophages (Fig. 1A, open bars).

Increasing the concentration of CF-hBD2 resulted in a linear increase in the accumulation of the peptide into macrophages, as indicated by a highly significant correlation between concentration and MFI (7 points, $R^2 = 0.99$, $p < 0.0001$). Furthermore, experiments were repeated with hBD2 linked to a different, uncharged

fluorophore (BODIPY), without discernable differences in behaviour, indicating that the presence of the fluorophore does not greatly affect binding or internalization (results not shown).

Flow-cytometric and TEM analyses of hBD2 interaction with iDC

The effects of hBD2 interaction with iDC was further investigated by correlating data from flow cytometry with TEM and optical and FTIR microspectroscopies (see below) under standardized conditions (1 μ M peptide, 30-60 minutes exposure in complete medium). iDCs were phenotypically characterized for specific co-stimulatory molecules and chemokine receptors in order to confirm the cell differentiation into immature (CCR6+) dendritic cells (DC-SIGN+) (Fig. 1S, supplementary material). Flow cytometric analyses indicated the presence of two subpopulations, R1 and R2 (Fig. 1C), respectively $70\% \pm 10$ and $30\% \pm 10$ of the total. R1 cells were morphologically more heterogeneous, with higher SS and FS values, indicating greater size and internal complexity than R2, which likely consisted of viable but incompletely differentiated cells. Phenotypical analysis confirmed a lower content of iDC markers for R2 (Fig. 1S supplementary material), which also showed a lower capacity to internalize labeled hBD2 (Fig. 1D). Naive and hBD2-exposed cells (unlabelled peptide) of both subpopulations were treated with FITC so as to monitor variations in protein content in terms of variations in mean fluorescence intensity. A statistically significant decrease ($10 \pm 5\%$ $p < 0.001$) in total protein was observed only for the R1 subpopulation after peptide treatment, with respect to untreated control (Fig. 1E).

Control and treated iDC samples were then investigated by transmission electron microscopy (Fig. 2). Their morphology resembles that of CD11c+ DC, characterized by microvillous projection of the plasma membrane, multilobulated nuclei and abundant vacuoles; unexposed cells were also characterized by the presence of numerous cytoplasmic vesicles (Fig. 2A) of approximately 200 nm diameter, with a dark, electron dense appearance, tightly packed at the level of the plasma membrane and also distributed in the cytoplasm. On exposure to hBD2 these appeared to release their content, while maintaining their size and integrity (Fig. 2B). At higher resolution, vesicle membranes in peptide treated cells presented discontinuities of 10-20 nm, which are consistent with the formation of some kind of large pore or channel.

SR-IRMS of iDC

This non-invasive method was used to detect variations in functional groups present in cellular macromolecules without the use of exogenous probes. iDCs, either untreated or treated with hBD2 for 30-60 minutes, were fixed on IR transparent calcium fluoride windows and first analyzed by acquiring spectra of single whole-cells. Up to 60 cells from each sample were analyzed, in order to gain comprehensive information on a statistically relevant number of samples. The vibrational pattern of these specimens is rather simpler than one would expect, considering the number of contributing biological molecules [22]. However, as can be seen from a representative infrared spectrum from an iDC cell (Fig. 3), key absorptions can be specifically assigned.

Whole-cell spectra were clustered into groups using a multivariate statistical algorithm that maximized intra-class similarities and inter-class differences [23], performed on the first derivatives of spectra in order to enhance spectral resolution and minimize base line variations. This was applied over the entire IR spectrum, from

3600 to 1100 cm^{-1} , for both control (Ct) and treated (T) cells. It fully succeeded in distinguishing two sub-populations, which on visual inspection correlated with substantial morphological differences (Fig. 4). The minor population (Ct-R2; ~30%) appeared smaller, with lack of pseudopodia and a heterochromatic nucleus, consistent with the R2 population observed in flow-cytometric experiments, while the main population (Ct-R1; ~70%) was formed by larger cells, with an extended cytoplasm and paler euchromatic nucleus, consistent with the R1 sub-population. The first derivatives of spectra for each of the R1 and R2 sub-populations differed principally in the bands centered at 1713 cm^{-1} and 1600 cm^{-1} (Fig. 4B), respectively associated with carbonyl stretching vibrations of nucleic acids and to variation in DNA base-pairing [16].

Peptide treated cells also consisted of two subpopulations with the same relative abundances (T-R2 and T-R1, data not shown), but while the treated R2 population did not cluster separately with untreated R2 cells when applying the classification algorithm over the two population taken together (Fig. 5A), the R1 population did (T-R1 and CT-R1 clusters are well separated in the dendrogram).

Spectral differences between treated and untreated R1 cells were observed principally in the spectral ranges 3020-2800 cm^{-1} and 1755-1475 cm^{-1} (Fig. 5B & 5C), relating to lipid/phospholipid bands as well as nucleic acid and protein bands, according to literature assignments (see legend to Fig. 3). They indicate significant alterations in the general lipid composition of R1 on exposure to hBD2, the variation being well above the sensitivity of the method (~ 0.005 a.u.), and greater than the standard deviation of averaged spectra. In particular, the reduced intensity for the band at 1736 cm^{-1} (Fig. 5B) is consistent with a decrement in phospholipid concentration relative to other signals, while variations in the 3000-2800 cm^{-1} region indicate an increase in CH_3 with respect to CH_2 moieties in lipids [24]. The band at 3012 cm^{-1} (Fig. 5C), on the other hand, was not altered, ruling out significant variation in acyl chain saturation. Furthermore, a moderate shift to higher wavenumbers of both symmetric and asymmetric C-H stretching bands (at 2852 and 2921 cm^{-1} respectively) is indicative of an alteration in lipid order [14].

Chemical distribution maps for selected treated and untreated R1 cells were then recorded with a spatial resolution of 5 μm . The intracellular chemical distributions for proteins, lipids and phospholipids in a selected naive cell are shown in Fig. 6A (top row), along with the optical image of the cell, for comparison, while the same information is provided for a selected hBD2-treated cell in Fig. 6B (top row). Protein signal mapping (P) is according to the Amide I band intensities at 1590-1705 cm^{-1} , lipids (L) according to the acyl chain stretching modes at 2800-3000 cm^{-1} , and phospholipids to the carbonyl ester absorptions at 1720-1760 cm^{-1} . The most appreciable difference upon peptide-treatment occurred for the intracellular distribution of phospholipids, with a relative decrease in the carbonyl ester IR signal, with respect to other signals, such that it falls below the detection limit in the cytoplasmic region.

Chemotactic activity of hBD2 on iDC

Chemotactic activity of hBD2 on iDC was evaluated via the modified Boyden chamber method, using the same immature dendritic cells as for the other experiments, collected from numerous different donors. In this respect, our study differs from others that either use CD34+ derived immature dendritic cells or HEK

transfected cells stably expressing human CCR6 [10]. Each preparation was extensively phenotyped before use. Moreover in our model, quantification of chemotaxis was carried out using a fluorimetric method that is likely more accurate than cell counting, and more sensitive as it measures both migrated and transmigrating cells.

iDC were derived from monocytes from 13 different donors, and levels of surface CCR6 receptor were varied by using different amounts of IL-4 [25]. The chemotactic activity exerted by 10 nM of the cognate ligand MIP-3 α correlated linearly with surface CCR6 expression (Fig. 7B, $p = 0.007$) although with a relatively poor correlation coefficient ($R^2 = 0.7$), which may be ascribed to a wide variation in chemotaxis due to donor differences [18]. Pretreatment of cells with anti-CCR6 antibody resulted in efficient neutralization of chemotaxis (Fig. 7A).

The chemotactic effect of hBD2 was determined at 1 μ M peptide [following literature indications [6] but in this case no correlation with the presence of surface CCR6 was observed ($R = 0.0006$, $p = 0.9986$) (Fig. 7C). The chemotaxis index showed an average increase of about 30% irrespective of the presence of surface CCR6 (Fig. 7A). Furthermore, the anti-CCR6 antibody neutralized the chemotactic effect of hBD2 only for iDC populations displaying a high level of surface receptor (chemotaxis reduced to 20%, not shown).

DISCUSSION

The effect of short-term exposure to hBD2 was evaluated on macrophages and immature dendritic cells as well as their monocyte precursors. In particular, binding and internalization of fluorescently labelled hBD2 (CF-hBD2 or BY-hBD2) was followed with the aim of determining whether the peptide acts essentially at the membrane level or if some is internalized and may thus also act on intracellular targets.

A simple protocol involving quenching of accessible fluorescein with the impermeant dye trypan blue (TB) [26] to separate contributions from surface-bound and internalized peptide clearly indicated that CF-hBD2 entered rapidly and efficiently into macrophage cells (Fig 1). This was confirmed by confocal microscopy, which shows punctuate peptide fluorescence both cortically and in the cytoplasm. The fact that peptide fluorescence was unvaried at 24 h, suggests that an endosomal pathway may not be involved, as fluorescein is inactivated in lysosomal conditions.

Uptake into macrophages occurred without significant permeabilization, in complete medium under physiologic salt concentrations. This is unlike the cidal activity of hBD2 towards bacterial cells, which is instead quite sensitive to the presence of salt and medium [5]. Blood derived monocytes were also able to bind and internalize CF-hBD2 but uptake was significantly lower, also taking their smaller size into account. iDC internalised a comparable amount of peptide to macrophages, but displayed a higher capacity to bind it externally. Our data thus indicate that three different types of APC display a differential capacity to rapidly bind and internalize hBD2, a process that is not accompanied by membrane permeabilization, and that macrophages showed the highest relative capacity to internalize the peptide, while iDCs bound the largest amount on the surface. It remains to be ascertained if internalisation is mediated by a receptor, an endocytotic process, or some form of self-promoted uptake through the membrane.

Given the efficient binding and internalization of hBD2 into iDC, we carried out a further, more detailed investigation of how this could affect different cellular parameters, correlating data from flow cytometry, and TEM, optical and FTIR microscopies, under standardized conditions, using cells from several different healthy donors as the model.

Flow cytometric analysis provided information on the morphological and functional differences between naive and hBD2-treated iDC from different donors and clearly indicated that the presence of two subpopulations, termed R1 and R2. The former was morphologically more heterogeneous, and formed by larger cells with a higher content of cytoplasmic organelles and vesicles. The less populated R2 likely consisted of a different subset of viable cells, as revealed by iDC marker analysis. These different populations also gave rise to different chemical infrared fingerprints, as revealed by IRMS (see below).

Exposure to hBD2 followed by FITC, a marker for protein content, indicated that only the R1 population, which significantly bound the peptide, showed a moderate but statistically significant decrease in protein content. Taken together, our data suggest that only the fully differentiated R1 subpopulation was responsive to short-term exposure to hBD2 treatment, in a manner that maintained its immature state but possibly activated an exocytosis or degranulation event, without compromising cell vitality. Transmission electron micrographs of untreated iDC showed the presence of dark, electron dense cytoplasmic vesicles, and on peptide treatment these appeared to release their content into the cytoplasm (Fig. 2). It has been reported that hBD2 can cause release of pruritogenic mediators from mast cells in a process that involves interaction with a G-protein coupled receptor, mobilization of cellular calcium and calcium-mediated degranulation [7], likely through vesicle fusion. We report that hBD2 can efficiently penetrate into iDC, and directly visualize the formation of defined pores or channels in granules, which could account for an osmotic swelling and favor expulsion of the intra-granular content via an alternative swelling/expulsion mechanism. The biological significance of this degranulation, and what role it plays in host defence, requires further characterization of the granules and their contents, which are as yet not well described in the literature.

To obtain further information on chemical changes occurring in peptide-treated cells that could accompany the above-mentioned internalization and degranulation events, samples were investigated by SR-IRMS and data analyzed both by multivariate statistical methods (for individual whole-cell) and by applying the univariate technique for single-cell intracellular functional-group mapping. We succeeded in establishing a correspondence between spectral differences and morphological features of the cells and confirmed the presence of two subgroups corresponding to the sub-populations observed using flow cytometry. Spectral differences mainly occurred in the 1755-1475 cm^{-1} region in bands related to carbonyl stretching vibrations associated with DNA (indicated by arrows in Fig.4B), a type of variation that has been assigned to the changes in chromatin structure required for transcription and linked to cell differentiation in hematopoietic cells [27], so it is in accordance with a differentiated R1 population and a less differentiated R2 population.

Cluster analysis of whole cell spectra further confirmed that only the R1 population responded to short-term treatment with hBD2, and displayed significant biochemical alterations, so that whole cell spectra no longer clustered with untreated

controls (Fig 5A). In particular, exposure to hBD2 induced significant alterations in the general lipid composition, suggesting a critical role of membranes in peptide induced cellular processes. Variations in the 1750-1600 and 3020-2800 cm^{-1} spectral regions indicate *i*) an increased lipid disorder, insufficient to affect the membrane integrity as cells remain PI negative, but which could be consistent with an increased membrane fluidity [14]; *ii*) variations in the CH_3/CH_2 ratio but no evidence of an alteration in the degree of lipid insaturation, consistent with a relative increase in cholesterol and sphingomyelin enriched regions with respect to phospholipids [24]. IRMS thus suggests that short-term exposure to non-toxic concentrations of hBD2 causes significant alterations to the membranes of iDC, an effect that had not previously been reported. This might also be related to the observed degranulation effects, as also suggested by high resolution SR-IRMS mapping.

Mapped cells from the R1 subgroup were chosen on the basis of cluster analysis of whole-cell spectra. Protein (P), lipids (L) and phospholipid (Ph) signals behaved somewhat differently upon treatment. For both treated and naive cells, the highest protein distribution located at the nucleus, consistent with the greater cell thickness and presence of histone proteins in this region. Similarly, chemical maps of lipids and phospholipids exhibit particularly high concentrations at the nuclear and perinuclear level, likely deriving from the membranes of the nuclear envelope and of the cellular organelles. However, while the overall distribution of proteins and lipids does not alter markedly in treated with respect to the naive cells, the phospholipid map shows a significant relative decrease in the Ph carbonyl ester signal in the cytoplasmic region, as can be better appreciated in the single color RGB maps (Fig. 6A and B, bottom rows). This effect was observed for all treated cells that were mapped, regardless of their derivation (buffies from 3 different donors), and supports a general rearrangement of the endomembrane system upon short exposure to hBD2.

Flow-cytometry, optical microscopy and IRMS data thus all converge to indicate significant changes in cellular features and membrane properties of iDC on short-term exposure to hBD2. These effects, and in particular alterations in the membrane system, could be linked to an altered cell motility, consistent with the reported chemotactic activity of hBD2 on iDCs [6]. It had initially been reported that this activity was due to interaction of hBD2 with the CCR6 receptor [6, 8], but this was later called into question [10, 28], so it might be due to other or additional processes, possibly also involving the observed alterations in membrane characteristics. We were thus led to investigate the chemotactic activity of hBD2, in comparison with that of the cognate chemokine for CCR6, MIP3 α .

Under our conditions, on the average, our results seemed to confirm those first reported by Yang et al. [6], indicating that 1 μM hBD2 induced a comparable chemotaxis to that induced by 10 nM MIP-3 α (Fig.7). However, while the chemotactic activity of MIP-3 α correlated well with the presence of surface CCR6, that of hBD2 was independent of the presence of surface receptor. Furthermore, while anti-CCR6 antibody always abrogated the effect of MIP-3 α , it had a neutralizing effect with hBD2 only for iDC populations displaying a high level of the surface receptor. We have previously reported this type of behavior also for a structurally simpler, artificial β -defensin [29], and this leads us to suppose that defensin-induced chemotaxis may be partly due to activation of CCR6, but that other mechanisms are also involved and in fact predominate if CCR6 is poorly exposed on the surface.

In fact, hBD2 is reported to chemoattract mast cells via another G-protein coupled receptor [30], and recently still other chemokine receptors, such as CCR2, have been reported to participate in chemotaxis by hBD2 [28]. Blood CD11c⁺ DC are reported to express this receptor [31]. Based on our results, we suggest that iDC may however not necessarily be activated by an agonist/receptor type interaction, but rather in a non-canonical manner, involving either interaction with the membrane surrounding the receptor, or alteration of properties such as membrane composition/fluidity. These considerations may help explain apparently conflicting reports in the literature [10,31-33], and also the fact that several different β -defensins, with quite diverse primary structures, and even linearized forms or truncated fragments with compromised secondary structure, all display apparently similar chemotactic behaviour on iDC [1,6, 28,29,31-34].

CONCLUSIONS

Taken together, our results lead to the following conclusions:

- i) hBD2 is able to interact rapidly with APC, leading to differential binding and cellular uptake.
- ii) iDC are most efficient in surface binding and macrophages in internalising peptide;
- iii) sub-cytotoxic concentrations of hBD2 trigger a rapid release of cytoplasmic vesicle content in iDC.
- iv) short term exposure to hBD2 also seems to trigger a generalized lipid rearrangement in iDC consistent with endomembrane re-organization and a possible increase in plasma membrane fluidity.
- v) hBD2-induced membrane variations may possibly correlate with increased cellular motility; accumulation of the peptide in the proximity of membrane-located receptors may favor a receptor-mediated activation of chemotaxis, while internalization of the peptide and/or its effects on membrane properties, might trigger this process in alternative ways, which need to be defined. This suggests a more complex mode of chemotactic action than was previously supposed.

It is tempting to speculate that membrane interaction of molecules like hBD2 on iDC, at non-toxic concentrations, may lead to accumulation within membrane patches around chemotactic receptors, thus stimulating their activities, while at the same time, internalization of the peptide and effects on internal mechanisms could help predispose the cell towards movement by altering its membrane characteristics, or for other functions related to the defensive role of iDC. In this context, the relevance of vesicle degranulation in iDCs, upon short-term exposure to hBD2, to their role in immunity requires further clarification.

ACKNOWLEDGEMENTS

This work was supported by the FVG LR26 regional grant R₃A₂ and Italian national grant PRIN 2007 (2007K9RFLS). F. Morgera acknowledges a PhD grant from Elettra Synchrotron Light Laboratory, and L. Creatti from Trieste University.

FIGURE LEGENDS

Fig.1: Peptide binding and internalization into monocytes, monocyte-derived macrophages (MDM) and immature dendritic cells (iDC) upon short exposure to hBD2.

A) Different cell types incubated with 1 μ M CF-hBD2 at 37 °C for 60 min with (open bars) or without (filled bars) Trypan Blue quenching. Data represent the mean \pm SEM of three independent experiments. Mean fluorescence intensity (MFI) from autofluorescence was less than 5 for all cell types; B) Representative confocal fluorescence microscopy image of a macrophage cell treated with CF-hBD2 for 60 min. Cortical actin (stained with phalloidin-TRITC, red) and CF-labelled peptide (green) are shown. C) Flow cytometric dot plot displaying forward (FS) and side scatter (SS) parameters for iDC. The R1 and R2 subpopulations are gated separately as indicated by the ellipses; D) Differential interaction of CF-hBD2 with the two cellular sub-populations, where the unshaded peak (MFI $\approx 10^1$) is the R2 gated population and the shaded peak (MFI $\approx 5 \times 10^2$) is the R1 gated population; E) Protein content determined by measuring FITC fluorescence, in untreated and hBD2-treated R1 and R2 subpopulations.

Fig.2: Transmission electron microscopy images of hBD2-treated iDC.

TEM images for untreated (A) and peptide-treated (B) cells are shown at increasing resolution (respectively 1.8K \times , 11K \times and 56K \times), highlighting the presence of electron dense vesicles in the cytoplasm of control iDC (A-1, 2, 3) and less electron dense vesicles upon peptide treatment (B-1, 2, 3). Vesicle size was approximately 200 nm. These images were selected from a large set of electron scans showing similar features.

Fig. 3: Representative IR spectrum from iDC cells and band assignment.

The most important cellular vibrational bands are indicated by arrows and assigned (ν = stretching modes, as = antisymmetric, s = symmetric)[taken from ref. 22]. The position of each absorption band and primary cell constituents to which the absorption modes are conventionally associated are: $\nu(\text{C-H})$ at $\sim 3010 \text{ cm}^{-1}$, olefins from unsaturated lipid acyl chains; $\nu_{\text{as,s}}(\text{C-H})$ at ~ 2960 and $\sim 2875 \text{ cm}^{-1}$, methyls from saturated lipid acyl chains; $\nu_{\text{as,s}}(\text{C-H})$ at ~ 2920 and $\sim 2852 \text{ cm}^{-1}$, methylenes from saturated lipid acyl chains; $\nu(\text{C=O})$ at $\sim 1737 \text{ cm}^{-1}$, esters from phospholipids; Amide I [80% $\nu(\text{C=O})$, 10% $\nu(\text{C-N})$, 10% N-H deformation] at $\sim 1655 \text{ cm}^{-1}$, mainly from protein peptide bonds. Protein side-chains and carbonyl stretching of nucleic acids may also occur in this region; Amide II [40% $\nu(\text{C=O})$, 60% N-H deformation] at $\sim 1543 \text{ cm}^{-1}$, protein main chain; $\nu_{\text{as}}(\text{P=O})$ at $\sim 1240 \text{ cm}^{-1}$, phosphate group from nucleic acids; $\nu_{\text{s}}(\text{P=O})$ at $\sim 1088 \text{ cm}^{-1}$, phosphate group from nucleic acids; band from $1300\text{-}900 \text{ cm}^{-1}$, complex network of vibrations from carbohydrates [$\nu(\text{C-O-C})$, (C-O-P) , (C-O) , (P-O-P)]. The attribution considers both the spectroscopic variables and the relative mass ratio of the most fundamental constituents of a eukaryotic cell: proteins (50% of the total cellular dry mass), nucleic acids (15%), carbohydrates (15%), lipids (10%) and minor constituents (10%) [taken from ref. 35].

Fig.4: FTIR single cell analysis on untreated iDC.

A) Dendrogram resulting from cluster analysis (Euclidean distances, Ward's algorithm) on first derivatives of spectra of untreated iDC (Ct = control) performed in the 1755-1475 cm^{-1} range, showing the discrimination between R1 (Ct-R1) and R2 (Ct-R2) cells. B) The inset panel B shows the averaged first derivative of spectra for Ct-R1 (black line) and Ct-R2 (grey line). The spectral line thickness is proportional to the standard deviation from the mean.

Fig. 5: FTIR single cell analysis on untreated and treated iDC.

A) Dendrogram resulting from cluster analysis (Euclidean distances, Ward's algorithm) on first derivatives of spectra of untreated (Ct) and treated (T) iDC performed in the 1755-1475 cm^{-1} range. Ct-R1 and T-R1 are discriminated into two distinct classes, while a clear class distinction could not be deduced for Ct-R2 and T-R2. (B) IR mean spectra representing carbonyl esters and Amide I region of untreated (black line) and treated (grey line) iDCs (top) and their subtraction spectrum (bottom). (C) IR mean spectra representing the acyl chain region of untreated (black line) and treated (grey line) iDCs (top) and their subtraction spectrum (bottom).

Fig.6: FTIR maps of hBD2-treated iDC.

A) Selected untreated cell from the Ct-R1 population and B) peptide-treated cell from the T-R1 population. The optical microscope images (left) correspond to the same cell for which the distribution maps of major cellular macromolecule absorptions was obtained (top rows): P = protein Amide I band; Ph = phospholipid carbonyl ester band; L = lipid acyl chain band. In these maps the color corresponds to signal intensity. In the RGB images (bottom rows) the red channel (left panel) relates to the protein Amide I signal and the green channel (middle panel) relates to the phospholipid carbonyl ester groups, the signal being proportional to color intensity. The blue channel (right panel) indicates their superposition showing areas of co-localization, and was obtained using the RG2B colocalization plugin of the ImageJ open source software (<http://rsbweb.nih.gov/ij/index.html>).

Fig.7: Chemotactic activity of hBD2 compared to MIP3 α .

Histograms representing percent migrated cells for hBD2 or MIP-3 α stimulated cells with respect to spontaneous cell migration. iDC were divided into three groups, those not presenting surface CCR6 (< 10%, denoted iDC/R⁻), those scarcely presenting surface CCR6 (10-60%, denoted iDC/R^{low}) and those strongly presenting surface CCR6 (>60%, denoted iDC/R^{high}). For MIP-3 α stimulated cells, the effect of pretreatment with a neutralizing antibody for CCR-6 is also shown. (B) Linear regression of % migration vs % cells presenting surface CCR6 for MIP3 α stimulated cells and (C) hBD2 stimulated cells. Plots were obtained with the GraPhpad InStat package and the solid line represents the regression while the dotted lines the confidence limits.

REFERENCES

1. Pazgier, M. Prahl, A. Hoover, D. M. and Lubkowski J. (2007) Studies of the biological properties of human beta-defensin 1. *J. Biol. Chem.* **282**: 1819-1829
2. Ganz, T. and Lehrer R.I. (1998) Antimicrobial peptides of vertebrates. *Curr. Opin. Immunol.* **10**(1):41-44
3. Yang, D. Liu, Z.H. Tewary, P. Chen, Q. de la Rosa, G. Oppenheim J.J. (2007) Defensin participation in innate and adaptive immunity. *Curr. Pharm. Des.* **13**(30):3131-3139
4. Lai, Y. and Gallo R.L. (2009) AMPed up immunity: how antimicrobial peptides have multiple roles in immune defense. *Trends Immunol.* **30**(3):131-141
5. Schröder, J.M. (1999) Epithelial antimicrobial peptides: innate local host response elements. *Cell. Mol. Life Sci.* **56**(1-2):32-46
6. Yang, D. Chertov, O. Bykovskaia, S.N. Chen, Q. Buffo, M.J. Shogan, J. Anderson, M. Schröder, J.M. Wang, J.M. Howard, O.M. Oppenheim J.J. (1999) Beta-defensins: linking innate and adaptive immunity through dendritic and T cell CCR6. *Science* **286**(5439):525-528
7. Niyonsaba, F. Hirata, M. Ogawa, H. Nagaoka, I. (2003) Epithelial cell-derived antibacterial peptides human beta-defensins and cathelicidin: multifunctional activities on mast cells. *Curr. Drug Targets Inflamm. Allergy.* **2**(3):224-231
8. Niyonsaba, F. Ogawa, H. Nagaoka, I. (2004) Human beta-defensin-2 functions as a chemotactic agent for tumour necrosis factor-alpha-treated human neutrophils. *Immunology* **111**(3):273-281
9. Boniotto, M. Jordan, W.J. Eskdale, J. Tossi, A. Antcheva, N. Crovella, S. Connell, N.D. Gallagher, G. (2006) Human beta-defensin 2 induces a vigorous cytokine response in peripheral blood mononuclear cells. *Antimicrob. Agents Chemother.* **50**(4):1433-1441
10. Soruri, A. Grigat, J. Forssmann, U. Riggert, J. Zwirner. (2007) Beta-Defensins chemoattract macrophages and mast cells but not lymphocytes and dendritic cells: CCR6 is not involved. *Eur. J. Immunol.* **37**(9):2474-2486
11. Vongsa, R.A. Zimmerman, N.P. Dwinell, M.B. (2009) CCR6 regulation of the actin cytoskeleton orchestrates human beta defensin-2- and CCL20-mediated restitution of colonic epithelial cells. *J. Biol. Chem.* **284**(15):10034-10045
12. Bhat, S. Song, Y.H. Lawyer, C. Milner, S.M. (2007) Modulation of the complement system by human beta-defensin 2. *J. Burns Wounds* **10**;5:e10
13. Dumas, P. Miller, L. (2003) The use of infrared microspectroscopy in biology and biomedical investigation. *Vib. Spectrosc.* **32**:3-21

14. Lewis, R.N. and McElhaney, R.N. (2007) Fourier transform infrared spectroscopy in the study of lipid phase transitions in model and biological membranes: practical considerations. *Meth. Mol. Biol.* **400**: 307-226
15. Jung, C. (2000) Insight into protein structure and protein-ligand recognition by Fourier infrared spectroscopy. *J. Mol. Recognit.* **13**: 325-351
16. Banyay, M. Sakar, M. and Gräslund, A. (2003) A library of IR bands of nucleic acids in solution. *Biophys. Chem.* **104**: 477-488
17. Sallusto, F. and Lanzavecchia, A. (1994). Efficient presentation of soluble antigen by cultured human dendritic cells is maintained by granulocyte/macrophage colony-stimulating factor plus interleukin 4 and downregulated by tumor necrosis factor alpha. *J. Exp. Med.* **179**:1109-1118
18. Conti, L. Cardone, M. Varano, B. Puddu, P. Belardelli, F. Gessani, S. (2008) Role of the cytokine environment and cytokine receptor expression on the generation of functionally distinct dendritic cells from human monocytes. *Eur. J. Immunol.* **38**(3):750-762
19. Dieu-Nosjean, M.C. Massacrier, C. Vanbervliet, B. Fridman, W.H. Caux, C. (2001) IL-10 induces CCR6 expression during Langerhans cell development while IL-4 and IFN-gamma suppress it. *J. Immunol.* **15**;167(10):5594-5602
20. Lupi, S. Nucara, A. Perucchi, A. Calvani, P. Ortolani, M. Quaroni, L. and Kiskinova, M. (2007) Performance of SISSI, the infrared beamline of the ELETTRA storage ring. *J. Opt. Soc. Am. B* **24**: 959-964
21. Gazi, E. Dwyer, J. Lockyer, N.P. Miyan, J. Gardner, P. Hart, C. Brown, M. Clarke, N.W. (2005) Fixation protocols for subcellular imaging by synchrotron-based Fourier transform infrared microspectroscopy *Biopolymers* **77**(1):18-30
22. Mantsch, H.H. (1996) *Infrared spectroscopy of biomolecules* (Mantsch, H.H. and Chapman, D., eds.) Wiley-LISS
23. Lasch, P. Kneipp, J. eds. (2008), *Biomedical Vibrational Spectroscopy* Wiley-Interscience
24. Dreissig, I. Machill, S. Salzer, R. Krafft, C. (2009) Quantification of brain lipids by FTIR spectroscopy and partial least squares regression. *Spectrochim. Acta A* **71**: 2069-2075
25. Carramolino, L. Kremer, L. Goya, I. Varona, R. Buesa, J.M. Gutiérrez, J. Zaballos, A. Martínez, A.C. Márquez, G. (1999) Down-regulation of the beta-chemokine receptor CCR6 in dendritic cells mediated by TNF-alpha and IL-4. *J. Leukoc. Biol.* **66**(5):837-844
26. Van Amersfoort, E.S. Van Strijp, J.A. (1994) Evaluation of a flow cytometric fluorescence quenching assay of phagocytosis of sensitized sheep erythrocytes by polymorphonuclear leukocytes. *Cytometry.* **17**(4):294-301

27. German, M.J. Pollock, H.M. Zhao, B. Tobin, M.J. Hammiche, A. Bentley, A. Cooper, L.J. Martin, F.L. and Fullwood, N.J. (2006) Characterization of Putative Stem Cell Populations in the Cornea Using Synchrotron Infrared Microspectroscopy. *Invest. Ophthalmol. Vis. Sci.* **47**(6): 2417-2421
28. Röhr, J. Yang, D. Oppenheim, J.J. Hehlhans T. (2010) Specific binding and chemotactic activity of mBD4 and its functional orthologue hBD2 to CCR6-expressing cells. *J. Biol. Chem.* **5**;285(10):7028-7034
29. Antcheva, N. Morgera, F. Creatti, L. Vaccari, L. Pag, U. Pacor S, Shai, Y. Sahl, H.G. Tossi, A. (2009) Artificial beta-defensin based on a minimal defensin template. *Biochem. J.* **15**;421(3):435-447
30. Niyonsaba, F. Iwabuchi, K. Matsuda, H. Ogawa, H. Nagaoka, I. (2002) Epithelial cell-derived human beta-defensin-2 acts as a chemotaxin for mast cells through a pertussis toxin-sensitive and phospholipase C-dependent pathway. *Int. Immunol.* **14**(4):421-426
31. Röhr, J. Yang, D. Oppenheim, J.J. Hehlhans, T. (2010) Human beta-defensin 2 and 3 and their mouse orthologs induce chemotaxis through interaction with CCR2. *J. Immunol.* **184**(12):6688-6694
32. Caux, C. Ait-Yahia, S. Chemin, K. de Bouteiller, O. Dieu-Nosjean, M.C. Homey, B. Massacrier, C. Vanbervliet, B. Zlotnik, A. Vicari, A. (2000) Dendritic cell biology and regulation of dendritic cell trafficking by chemokines. *Semin. Immunopathol.* **22**(4):345-369
33. Taylor, K. Rolfe, M. Reynolds, N. Kilanowski, F. Pathania, U. Clarke, D. Yang, D. Oppenheim, J. Samuel, K. Howie, S. Barran, P. Macmillan, D. Campopiano, D. Dorin, J. (2009) Defensin-related peptide 1 (Defr1) is allelic to Defb8 and chemoattracts immature DC and CD4+ T cells independently of CCR6. *Eur. J. Immunol.* **39**(5):1353-1360
34. Rohrl, J. Yang, D. Oppenheim, J.J. and Hehlhans, T. (2008) Identification and Biological Characterization of Mouse beta-defensin 14, the orthologue of human beta-defensin 3. *J. Biol. Chem.* **283**: 5414-5541
35. Alberts, B. Bray, D. Lewis, J. Raff, M. Roberts, K. Watson, J.D. (1994) *Molecular Biology of the Cell*, 3rd Edition (Robertson, M., Adams, R., Goertzen, D., Cobert, S.M. ed.) Garland Publishing Inc., New York, USA

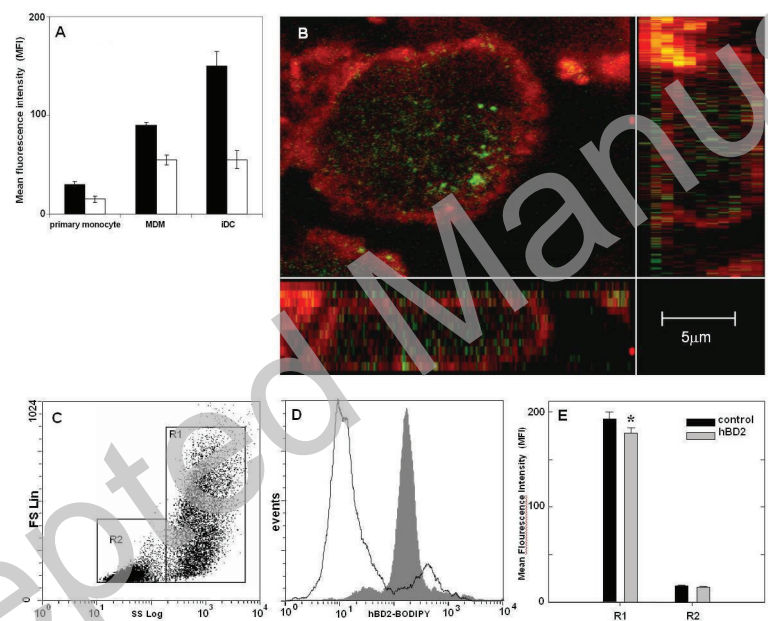


Figure 1

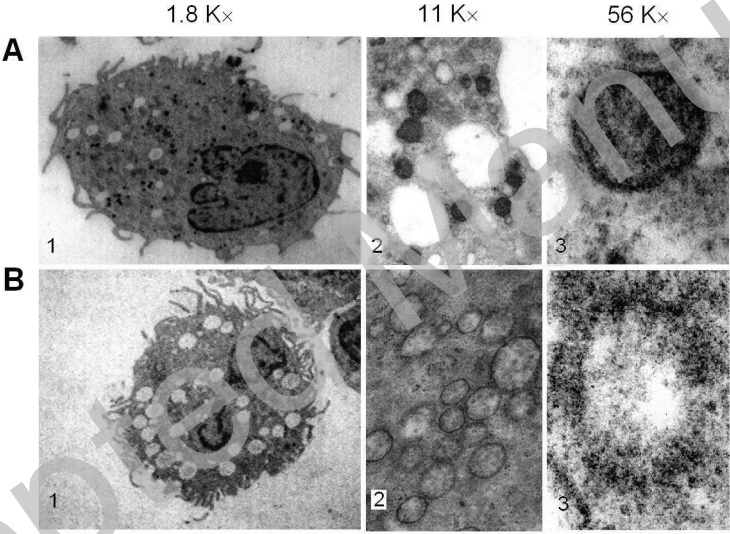


Figure 2

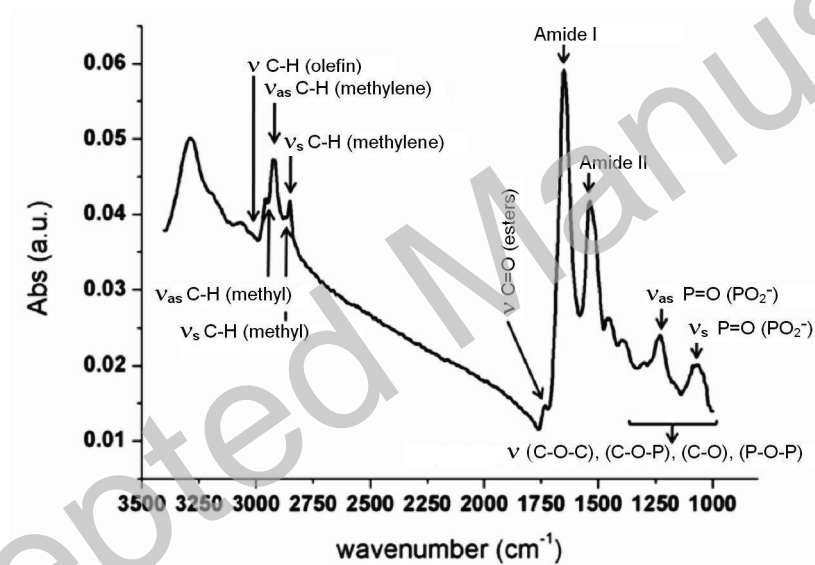


Figure 3

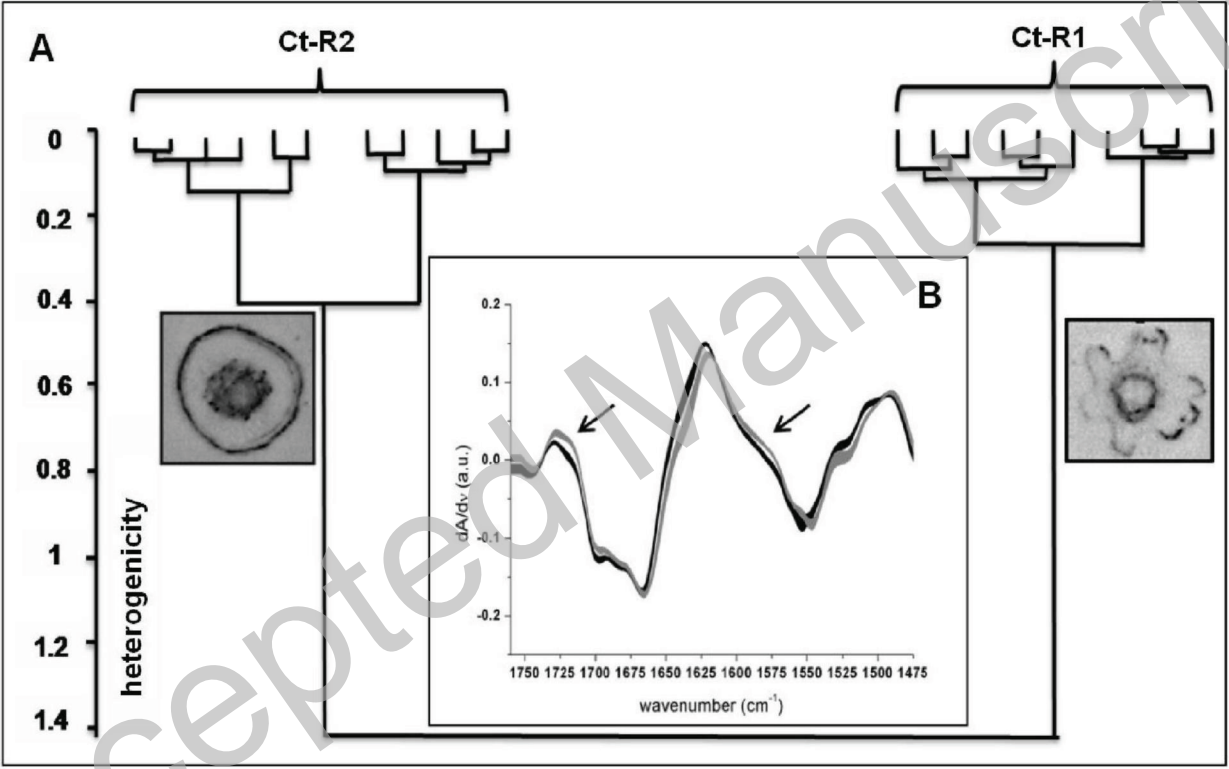


Figure 4

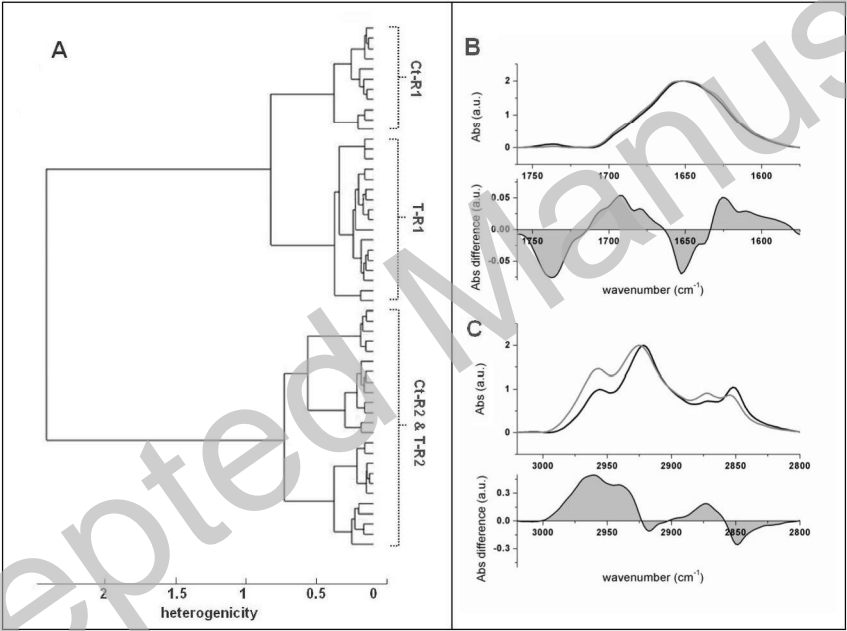


Figure 5

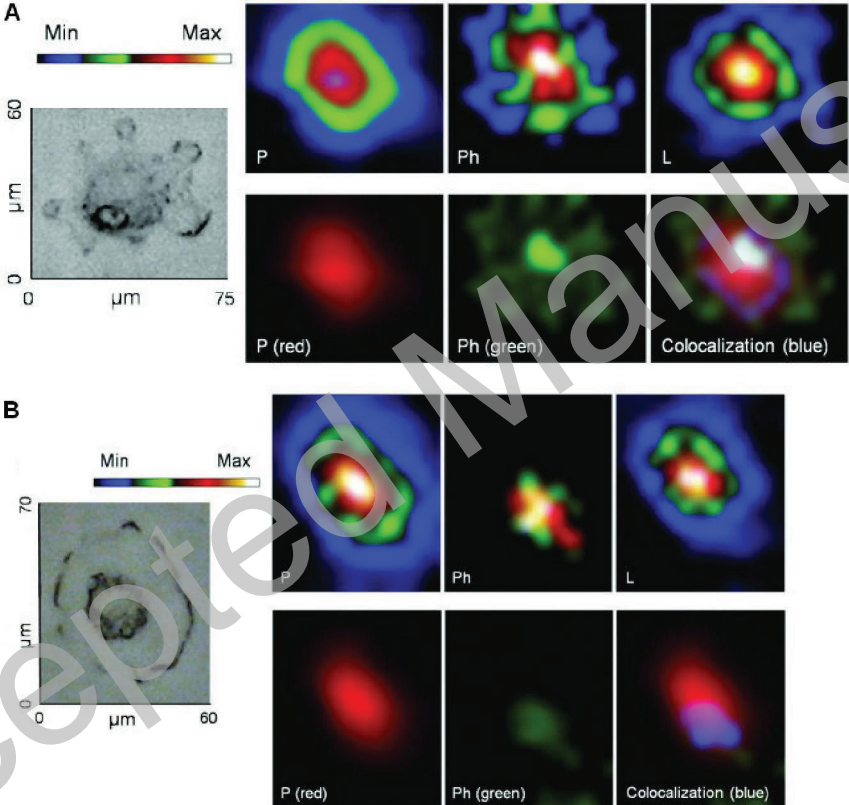


Figure 6

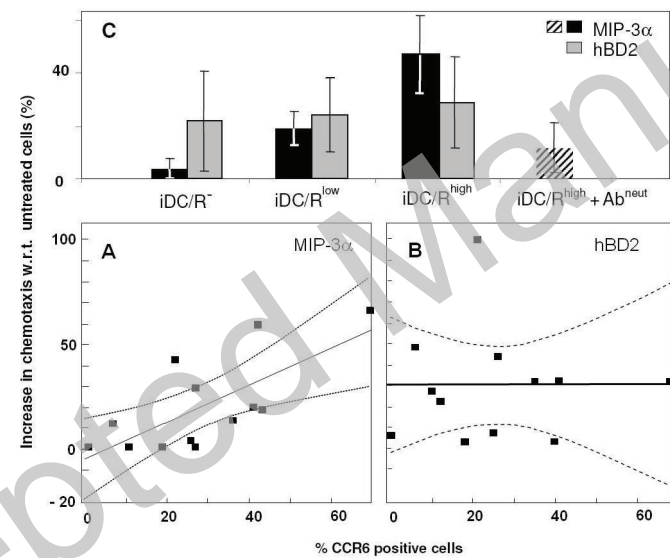


Figure 7